Journal of Power Sources 267 (2014) 366–379

Contents lists available at ScienceDirect

Journal of Power Sources

journal homepage: www.elsevier.com/locate/jpowsour

A new method of accelerated life testing based on the Grey System Theory for a model-based lithium-ion battery life evaluation system

Weijun Gu [a, b, *], Zechang Sun [a, b], Xuezhe Wei [a, b], Haifeng Dai [a, b]

[a] National Fuel Cell Vehicle & Powertrain System Research & Engineering Center, No. 4800 Caoan Road, Shanghai 201804, China
[b] School of Automotive Studies, Tongji University, No. 4800 Caoan Road, Shanghai 201804, China

HIGHLIGHTS

- Present a new method for accelerating battery life test.
- Establish a residual grey model combining the aging law to describe the battery life trend.
- Predict the battery cycle life with a small number of testing samples.

ARTICLE INFO

Article history:
Received 18 September 2013
Received in revised form
18 April 2014
Accepted 20 May 2014
Available online 4 June 2014

Keywords:
Accelerated life testing
Grey model
Performance degradation
Lithium-ion battery

ABSTRACT

The lack of data samples is the main difficulty for the lifetime study of a lithium-ion battery, especially for a model-based evaluation system. To determine the mapping relationship between the battery fading law and the different external factors, the testing of batteries should be implemented to the greatest extent possible. As a result, performing a battery lifetime study has become a notably time-consuming undertaking.

Without reducing the number of testing items pre-specified within the test matrices of an accelerated life testing schedule, a grey model that can be used to predict the cycle numbers that result in the specific life ending index is established in this paper. No aging mechanism is required for this model, which is exclusively a data-driven method obtained from a small quantity of actual testing data. For higher accuracy, a specific smoothing method is introduced, and the error between the predicted value and the actual value is also modeled using the same method.

By the verification of a phosphate iron lithium-ion battery and a manganese oxide lithium-ion battery, this grey model demonstrated its ability to reduce the required number of cycles for the operational mode of various electric vehicles.

1. Introduction

The evaluation of the lifetime of a lithium-ion battery is an important issue for the development and expansion of the use of Electric Vehicles (EVs). An effective evaluation system can not only diagnose the causes of battery failure and potential danger, thereby ensuring the vehicle's security, but also regulate the use of an EV to extend the battery life and reduce the relative cost of the battery.

According to the objectives of the assessment, the current battery life evaluation systems mainly include the actual life testing under typical working conditions and a model-based method of evaluation.

The primary purpose of the actual life tests is to assess whether the battery can meet the requirements of the typical vehicle applications. For example, the FreedomCAR program has proposed that the battery life of up to 15 years and 300,000 cycle numbers within a shallow State of Charge (SoC) window be the goal for Hybrid Electric Vehicle (HEV) applications. In anticipation of such battery performance, many similar testing specifications and processing methods of experimental data have been developed worldwide [1]. Although this type of application-driven evaluation approach can provide a reference for battery selection and vehicle design, it is difficult to

* Corresponding author. National Fuel Cell Vehicle & Powertrain System Research & Engineering Center, No. 4800 Caoan Road, Shanghai 201804, China. Tel.: +86 21 69589091.
E-mail address: guweijun76718@hotmail.com (W. Gu).

http://dx.doi.org/10.1016/j.jpowsour.2014.05.103
0378-7753/

estimate the State of Health (SoH) of a battery in use, which is more reliant on the model-based evaluation methods.

For the model-based evaluation approaches, the primary methods are the aging mechanism model, the semi-empirical model and the data-driven model. Various other models have emerged in some available instances. Based on the porous electrode theory, Ramadass et al. have developed a first principles capacity fading model for a lithium-ion battery in Ref. [2], and a commercial simulation tool has been developed by COMSOL 3.5 based on this model. Models based on a similar mechanism have also been developed in Refs. [3–5]. This type of model is primarily based on the principles of the particle transportation process and the reaction process, which were generalized by John Newman's team in Refs. [6,7]. The core of this type of model is the establishment of the variation law of the specific internal or external eigen-parameters during the entire aging process, which is obtained from some simulation work or from numerous accelerated life testing results under various working conditions. Those degradation laws are also the basis of the empirical and semi-empirical lifetime model. Among such models, Bloom et al. [8] characterized the power degradation law of a lithium-ion battery with the power function of the time of use, and their fitting result of the exponent of time approached 0.5. Thereafter, John Wang et al. [9] introduced this type of model structure into the modeling of the capacity fading. Thomas et al. in Ref. [10] and Wright et al. in Ref. [11] reported that such an empirical model can be used to predict the cycle life under the variable stress conditions and the calendar aging conditions. This type of empirical or semi-empirical lifetime model is concise compared with the mechanism model and has become highly feasible for use in EV applications. However, the unknown parameters, such as the weight factor of each external factor, still rely on a huge number of accelerated life testing results. Additionally, the inherent inconsistency between the same type and the same batch of batteries determine the necessity to repeat the same testing cycle several times. Compared with these two types of lifetime models, it is even more necessary to accumulate sufficient experimental testing results for the data-driven evaluation method. The data-driven model is generally based on the statistical method, which relies on a good probability distribution. Thus, whether it is established by the adaptive filtering method [12] or the Monte Carlo simulation method [13,14], these approaches all require sufficient data sets as their modeling basis. As long as these data sets can at least cover the dynamic range of the battery life characteristic, the data-driven models can possess high credibility in their use for lifetime evaluation for a lithium-ion battery. The larger the dynamic range of the sample data that can be covered, the higher is the accuracy of the prediction model that can be obtained. Thus, it is necessary to study accelerated life testing procedure used to obtain the performance data samples when the model-based evaluation method is used.

In capacity fading, for example, the primary task of the cycle life testing process for the model-based lifetime evaluation method is recording the actual capacity at different life state until the pre-specified ending indicator, such as 80% of the initial capacity, is achieved. With the high quality material now being developed for a lithium-ion battery, the data acquisition of battery performance degradation has become an increasingly time-consuming process. Even if accelerated lifetime testing is used, the complete testing matrices containing generally accepted external factors, such as discharge rate, DoD and temperature, should be pre-specified [8–10,15]. Additionally, to determine the relationship between the external factors and the attenuation law, the testing matrices should measure more battery degradation characteristics. Thus, it is more reasonable to shorten the cycle numbers for each testing item than to reducing the number of testing items in the testing matrices. To obtain the approximate numbers of cycles using a small amount of experimental data, there are two primary issues that must be solved: one is the small number of lifetime testing samples, and the other is the complicated coupling between the effects of the external impact factors and the degradation results.

To solve these two problems, a new accelerated method for model-based evaluation system is presented in this study, which can be used to predict the cycles resulting in the pre-specified life-ending indicators and thus shorten the testing numbers correspondingly. Based on this model, no testing item is abandoned, and only a number of testing samples over a relative small cycle range are required. The entire method is still a data-driven method in nature, while also having the ability to predict the battery performance degradation law for any specific working condition; however, this method is not a battery lifetime model because the parameters in the prediction model change for different working conditions. Another feature is the method of experimental data smoothing in our study, which also refers to some general recognized cycle life model structure.

As for the battery performance degradation, the mechanism of the external impact factors is indefinite, but the fading trend of the performance caused by these external factors is determined. This type of system can be called a "grey causes and white results" system, which can be described by Grey System Theory [16,17]. Our study is just based on the Grey Model (GM) established by Julong Deng. The GM exhibits high accuracy even if the number of testing samples is very small. Thus, the GM method is proper for solving the issues being confronted in the accelerated lifetime testing.

The remaining parts of the paper are organized as follows. In first section, a detailed introduction of the testing sample, protocol and contents is presented. Next, we analyze the characteristics of a battery life system to translate this system into the grey system, while concurrently introducing the GM. Combining the GM system and the battery lifetime degradation law, a residual GM (1, 1) model based on the battery aging mechanism is subsequently established. Next, the verification of this model by predicting the characteristics of a manganese oxide lithium-ion battery and a phosphate iron lithium-ion battery is presented in detail. Finally, we provide a number of conclusions based on the results of our study.

2. Experiment

The battery cells used in our study include two typical types of lithium-ion batteries, i.e., a high-power manganese oxide lithium-ion battery and a phosphate iron lithium-ion battery; the detailed information of both of these batteries is listed in Table 1. Additionally, the testing facilities are tabulated in Table 2, and the testing bench is described in Fig. 1.

In our study, we designed the multi-factor testing matrices as listed in Refs. [8,9] for the manganese oxide lithium-ion battery, which can be considered as simulating the conditions of a Battery Electric Vehicle (BEV) in driving mode, and the testing items are sufficient for creating a cycle life model as described in Refs. [8–11].

Table 1
Specification of the testing samples.

Manganese oxide lithium-ion battery		Phosphate iron lithium-ion battery	
Parameters	Value	Parameters	Value
Rated capacity (Ah)	8	Rated capacity (Ah)	8
Rated voltage (V)	3.7	Rated voltage (V)	3.2
Charge cut-off voltage (V)	4.2	Charge cut-off voltage (V)	3.7
Discharge cut-off voltage (V)	2.7	Discharge cut-off voltage (V)	2.5
Maximum pulse charge/discharge rate (C)	25 (20 s)	Maximum pulse charge/discharge rate (C)	25 (20 s)

Table 2
Detailed information of the testing facilities.

Facilities	Specification	Function
Ambient chamber	Partner PHV1402	To emulate the environmental temperature under which the battery cells work
Battery cycler	Arbin EVTS-IGBT	To load the current cycles
Electro-chemical workstation	Maccor 4300	To calibrate the capacity of the battery cells
Computer and Ethernet router	–	To control the test procedures, and record the experiment data

Table 3
The cycle life accelerated testing matrices for Manganese oxide lithium-ion battery under BEV working mode.

Testing items	Fixed factors		Adjusted factors
Degradation under different discharge rates	DoD (%)	100	Discharge rate (C)
	Temperature (K)	313	1, 2, 3, 4, 5
Degradation under different DoDs	Discharge rate (C)	1	DoD (%)
	Temperature (K)	313	100, 80, 60, 40, 20
Degradation under different temperatures	DoD (%)	100	Temperature (K)
	Discharge rate (C)	1	293, 303, 313, 323

However, for the phosphate iron lithium-ion battery, we reduced some testing items under the BEV mode due to the longer cycle life of the testing samples, and some testing items of the HEV operational mode were added to validate our method.

The accelerated lifetime testing includes cycle life testing and the performance calibration testing.

2.1. Cycle life testing

2.1.1. BEV mode

For manganese oxide lithium-ion battery under BEV mode, the testing items are listed in Table 3. The entire testing process is divided into three cases to evaluate the effect of the discharge rate, DoD and ambient temperature on the battery performance. For each testing item, we charge the battery in the constant current–constant voltage (CC–CV) mode, for which the charge rate in CC stage is set to 1/2 C and the cut-off current rate in CV stage is set to 1/100 C. Concurrently, we discharge the battery in the constant-current (CC) mode, for which the discharge rates of each testing item are listed in Table 3. The values of the corresponding cut-off voltage in the charge/discharge process are listed in Table 1. A similar protocol is specified for the phosphate iron lithium-ion battery cell under BEV mode, with the main difference being the value of the charge/discharge cut-off voltage, which also is listed in Table 1. The detailed information of the testing items is listed in Table 4.

2.1.2. HEV mode

For the phosphate iron lithium-ion battery cell under HEV mode, an operating point based on the SoC is pre-set. We first charge the battery to this pre-specified SOC in CC mode, with the

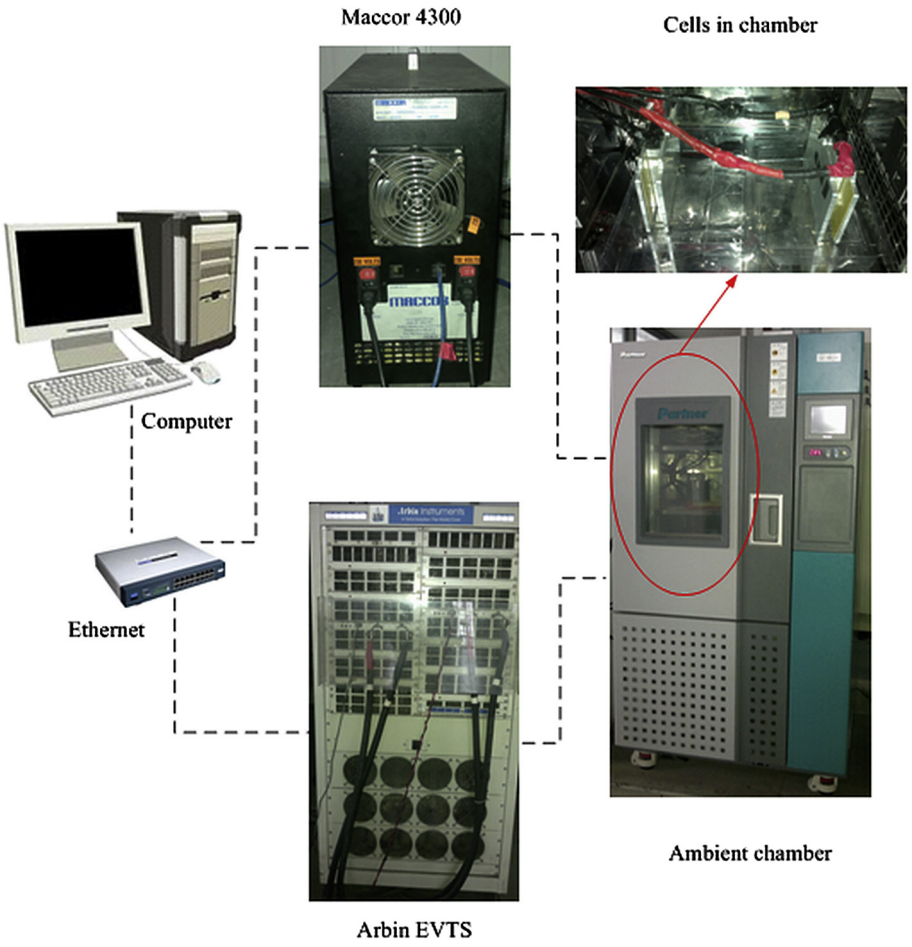

Fig. 1. Testing bench used for the accelerated life tests.

Table 4
The cycle life accelerated testing matrices for the Phosphate iron lithium-ion battery under BEV working mode.

Testing items	Discharge rate (C)	DoD (%)	Temperature (K)
1	2	100	303
2	2	100	323

charge rate in the CC stage set to 1/2 C. Next, the current profile during the charge and discharge cycle is varied around this operating point. The pre-set SoC operating point and the ambient temperature of each testing item are listed in Table 5, and the cycle profile is shown in Fig. 2. To reduce the SoC drifting induced by the sampling accuracy of the testing devices, the battery is fully charged and discharged after a number of cycles.

2.2. Calibration testing

Capacity is the indicator of battery performance degradation in our study. To remove the effects of the environment on the measured value, all the samples are calibrated under the same ambient temperature, i.e., 25 °C, and operated in the full charge and discharge mode. The testing protocol of the charge mode is identical with that of the cycle life testing described in 2.1. The current rate is uniformly set to 1/2 C for all the samples in the discharge steps, and the other protocols of the discharge mode remain unchanged.

3. Methodology

3.1. Analysis of the battery life system

For the battery cycle life, there are many external factors that affect the battery performance, and the relationship between these factors is not decoupled. As described in Fig. 3, the testing sample of a high-power manganese oxide lithium-ion battery working under the testing condition of 6.25 C discharge rate, 70% of DoD and 25 °C temperature has a higher cycle performance compared with the testing sample with 1 C discharge rate, 100% of DOD and 30 °C, which makes it difficult to interpret which external impact factor plays a more important role in the battery aging process. Even if the level of these external factors remains constant, the mode of operation also makes a great difference in the battery fading rate. As shown in Fig. 4(a) and (b), the capacity fading rate becomes faster when a rest step between each different discharge stage is added. Similarly, it is also difficult to explain the reason that the cycle life of the battery will be improved substantially when the appropriate external connection stress is applied to the testing sample, as shown in Fig. 5. In summary, due to the complicated aging mechanism, it is difficult to assign a specific fading form to one or some identified external factors, especially when the external impact factors and the mode of use are all at different levels. However, the fading trend is irreversible under the effects of these external factors throughout the life process. From this point of view, the cause of the battery degradation is uncertain, but the trend of battery degradation remains unchanged; as a result, this type of system can be regarded as a Grey System.

Table 5
The cycle life accelerated testing matrices for Phosphate iron lithium-ion battery under HEV working mode.

Testing items	SoC (%)	Temperature (°C)
1	50	40
2	65	50
3	50	50

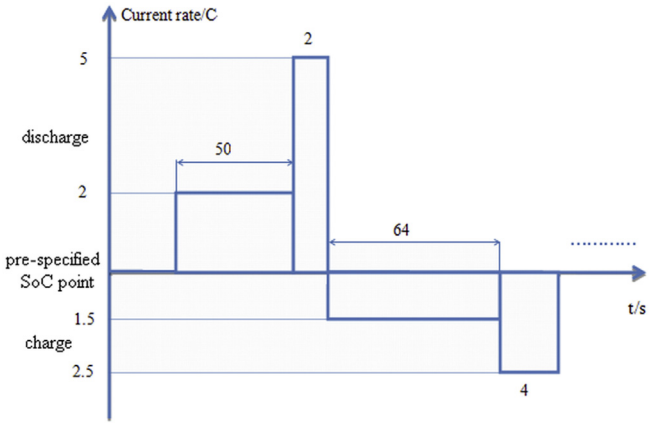

Fig. 2. The charge and discharge current profile waves around a pre-specified SoC point under the HEV cycle operation mode.

Among the data-driven methods, the study of the statistical methods and fuzzy mathematics is also focused on uncertain systems; however, the Grey System is different from these two systems. The basis of a statistical method is a large number of samples, which is the constraint of battery life modeling, subjected to a certain typical distribution. Conversely, the Grey System focuses on an uncertain system with the characteristics of a small sample and poor information [16,17]. Fuzzy Mathematics applies to the system with cognitive uncertainty, i.e., neither the internal excitation nor the external response of this type of system is very clear. For the battery life prediction system, the internal aging mechanism that leads to a specific type of battery degradation is not clear, but the degree of this type of battery fading can be quantified by some measurable index, such as capacity or internal resistance. Thus, from the perspective of the data-driven method, the Grey System is more suitable for use in a battery life system, due to the small number of life samples, the complicated aging mechanism and the coupling between the different external impact factors.

3.2. Introduction of the GM (1, 1) model

3.2.1. Definition of the GM (1, 1) model

A random time series must contain some inherent tendency for a specific event to some extent [16,17]. Based on this point of view, the Grey Method uses some smoothing algorithm, such as accumulated generating operation (AGO), to process the raw data to reduce their stochastic degree, thus enabling the change of the initial process within a long time range to be described by the newly generated data series. Based on the GM (1, 1) model, which is an important branch of the Grey System Theory, the development law of the uncertain system can be revealed, and the future state of this system can be predicted by this established GM model.

The block diagram of the GM (1, 1) model is drawn in Fig. 6.

The defined model of GM (1,1) is:

$$x^{(0)}(k) + az^{(1)}(k) = b \tag{1}$$

Eq. (1) can be changed into

$$b - az^{(1)}(k) = x^{(0)}(k) \tag{2}$$

where

$$x^{(0)} = \left(x^{(0)}(1), x^{(0)}(2), \cdots, x^{(0)}(n)\right) \tag{3}$$

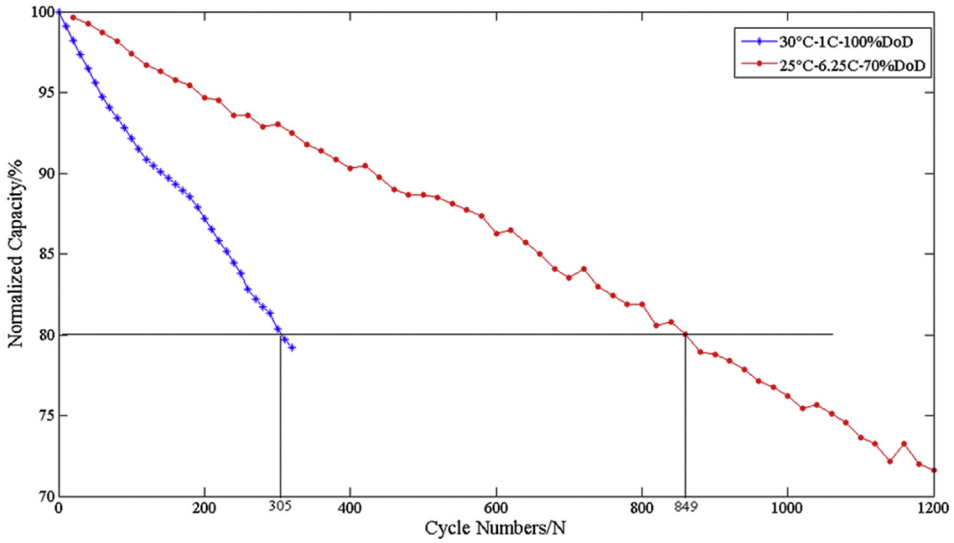

Fig. 3. Comparison of the capacity fading rate between two testing items with different levels of external impact factors.

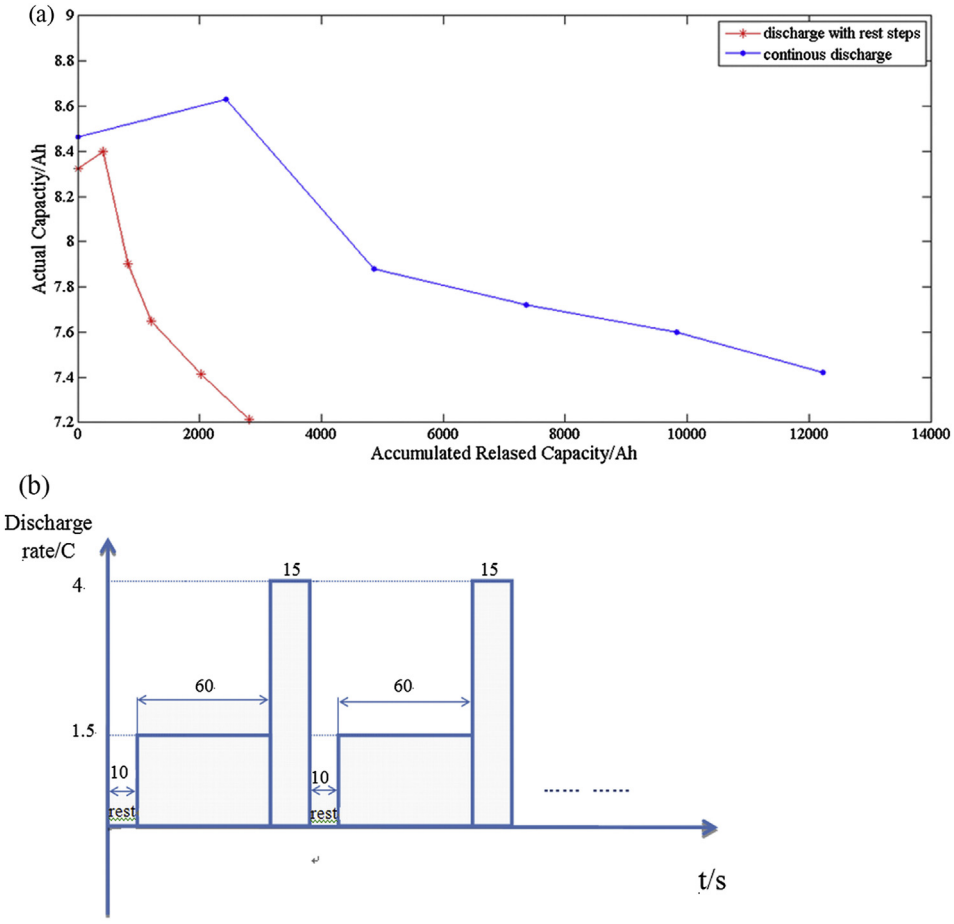

Fig. 4. (a) Horizontal axis represents the accumulated capacity released by the testing samples, and the vertical axis is the actual capacity corresponding to this battery life stage. The charge condition is identical for the two cycle modes, and the discharge mode is different for each case. The discharge rate for the continuous discharge mode is set to 2 C and the discharge profile for the other discharge mode with some rest steps is shown in (b) The discharge rate profile applied to the discontinuous discharge mode with some rest steps, but the average of the discharge rate is also 2 C.

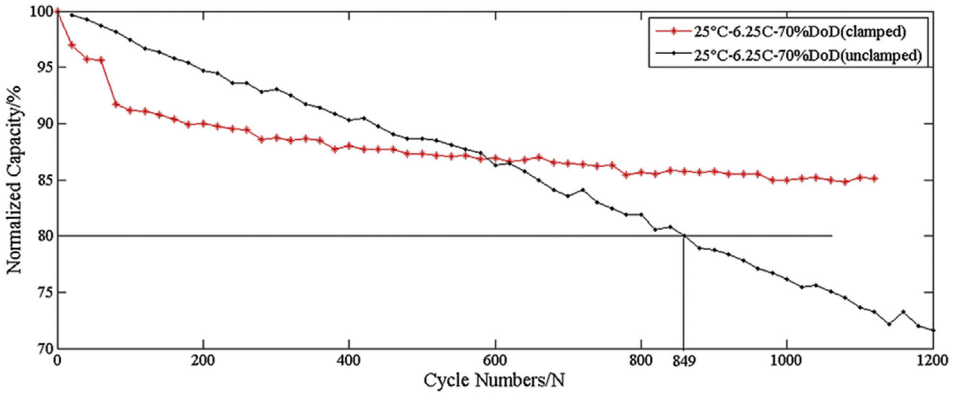

Fig. 5. Comparison of the capacity fading rate under different fixation modes, with the other testing conditions being identical.

is the raw data series, where a is known as the development coefficient, and b is known as the endogenous control coefficient.

$$x^{(1)} = \mathrm{AGO}x^{(0)} \tag{4}$$

$$z^{(1)}(k) = \mathrm{MEAN}x^{(1)}(k) \quad k = 1, 2, \cdots, n \tag{5}$$

where the definition of AGO is

$$x^{(1)}(k) = \sum_{m=1}^{k} x^{(0)}(m) \quad k = 1, 2, \cdots, n \tag{6}$$

and MEAN is

$$z^{(1)}(k) = 0.5x^{(1)}(k) + 0.5x^{(1)}(k-1) \quad k = 2, \ldots, n \tag{7}$$

The principle of GM (1, 1) can be described by Fig. 6 and Eq. (2). In Fig. 6, the variable b represents the ambiguous influence mode of the external impact on the development of an event, and $x(0)$ represents the real value of this event. The diagram describes the law of causality from the input to the output. Because the variable b is obtained from some identification method, such as the Least Squares Method (LMS), it is known as the grey causes. Additionally, because $x(0)$ is the actual observable variable, it is known as the white result.

3.2.2. Identification of the parameters for the GM (1, 1) model

The essence of the modeling is to establish coefficients in the differential Eq. (2). First, some intermediate parameters are introduced.

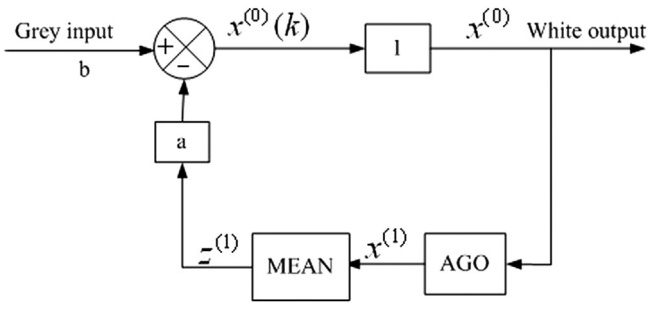

Fig. 6. Block diagram of the GM (1, 1) modeling process.

$$C = \sum_{k=2}^{n} z^{(1)}(k) \tag{8}$$

$$D = \sum_{k=2}^{n} x^{(0)}(k) \tag{9}$$

$$E = \sum_{k=2}^{n} z^{(1)}(k)x^{(0)}(k) \tag{10}$$

$$F = \sum_{k=2}^{n} z^{(1)}(k)^2 \tag{11}$$

Next, the required parameters a and b in GM (1,1) are indentified by the LMS method:

$$a = [CD - (n-1)E] \Big/ \left[(n-1)F - C^2\right] \tag{12}$$

$$b = (DF - CE) \Big/ \left[(n-1)F - C^2\right] \tag{13}$$

The boundary conditions of the GM (1, 1) model are described below.

For the time series

$$x = (x(1), x(2), \cdots, x(n)) \tag{14}$$

we define the progressive proportion $\sigma(k)$ of the time series

$$\sigma(k) = x(k-1)/x(k) \tag{15}$$

As long as the domain of parameter a and $\sigma(k)$ in the GM (1, 1) model are within the range of $(-2/(n+1), 2/(n+1))$ and $(\exp(-2/(n+1)), \exp(2/(n+1)))$, respectively, these two parameters are solvable, and the model of GM (1, 1) is meaningful. Due to the fact that the effective domain of the $\sigma(k)$ can also guarantee the effective a, it is necessary to verify the solvable domain for $\sigma(k)$ and design some smoothing method for the raw time series when the $\sigma(k)$ does not meet the requirements.

In general, the modeling process of GM (1, 1) can be summarized as follows.

① Boundary conditions verification.
② Data smoothing.
③ GM (1,1) modeling.
④ Forecasting.
⑤ Model accuracy validation.

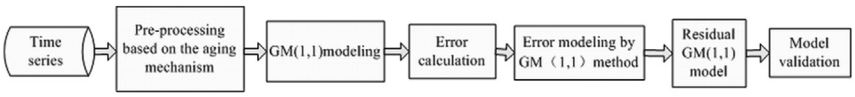

Fig. 7. The flow chart of the combined residual GM (1, 1) model for battery life ending prediction.

3.3. Characteristics of grey prediction for a battery life system

The advantage of the Grey Method lies in its ability to reflect the trend of the data series without requirements for prior knowledge and little requirements for the small numbers of the sample data, which makes it attractive for use in a battery life evaluation system. However, the sample data will exhibit some new trend with the continuous performance degradation, and the error between the experimental result and the prediction value will increase, especially if the data used for GM (1, 1) modeling is sampled within a relative minor range, in which the degradation of the battery performance is very slight. Thus a single GM (1, 1) model may not obtain improved prediction accuracy. While the same GM (1, 1) method also can be used to model this part of the error, which can be named the residual GM (1, 1) model, for the compensation of this deviation caused by the new degradation trend. Concurrently, some data smoothing methods, which are based on the general recognized cycle life model structure of a lithium-ion battery, have also been introduced in our study; in this way, the accuracy of the predicted value resulting in a specific ending indicator is further improved.

3.4. The combined residual GM (1, 1) model for battery life ending prediction

To improve the prediction accuracy of the GM (1, 1) model for a battery life evaluation system, it is necessary to adopt a smoothing method for the experimental data based on the battery life aging mechanism. To predict the number of cycles to shorten the testing time of the battery life evaluation, we impose the square root operation on the raw sample data before we establish a residual GM(1,1) model, due to the common recognition of the linear relationship between the capacity fading rate and the square root of the usage time ($t^{1/2}$) [8–10].

The flow chart of the residual GM (1, 1) modeling for accelerated life testing is shown in Fig. 7. The detailed modeling process is described below.

(1) Let the raw data series sampled in a narrow testing range relative to the complete cycle numbers for testing item i specified in the testing matrices be

$$T_i = [Si_1, Si_2, Si_3, \ldots S_{ij}, \ldots S_{in}] \tag{16}$$

$$S_{ij} = \left(\text{capacity}_{ij},\ \text{cycle}_{ij}\right) \quad (j = 1, 2, \ldots n) \tag{17}$$

where the cycle number of each sample point, i.e., cycle_{ij}, may be distributed evenly or unevenly. The entire method is based on these small number of performance data, which are obtained in the early cycle numbers relative to the entire accelerated life testing. Thus, the sampling range in which the performance data have been collected also plays an important role for the prediction accuracy. Accordingly, the concept of the Accelerated Ratio (AR) is defined in Eq. (18)

$$\text{AR} = \text{the experienced cycle numbers for sampling performance data/the entire cycle numbers achieved at the battery end of life} \tag{18}$$

The value of AR can be used not only to guide the subsequent GM (1, 1) modeling process for the selection of the sample size but also to assess the effectiveness of this accelerated method.

(2) The interpolation operation is implemented on the sampling series [(capacity_{ij}, cycle_{ij})] (j = 1, 2, … n) to obtain the interpolation series of the cycle number, where the interpolation interval is defined as a small constant, such as 1% of the initial capacity, and the domain of the interpolation is designated by the life ending indicator, such as 80% of the initial capacity. The purpose of the interpolation operation is to ensure that sample of cycle number for GM (1, 1) modeling is distributed evenly in the time domain. Subsequently, the square root operation is implemented on these interpolation cycle values, and the boundary conditions verification operation of the GM (1, 1) model is simultaneously implemented.

(3) Intercept the cycle number time series obtained in step 2 from the first item as the modeling samples $x(0) = [cn_1, cn_2, \ldots cn_k, \ldots cn_m]$, where m is the larger one between the constant 5 and the serial number that corresponds to the value closest to the last one in the series T_i. And then the GM (1, 1) model can be established by the time series $x(0)$, with the eigen-parameters of the GM model identified based on Eq. (8) to Eq. (13). Note that the model structure is not delicately designed for a battery life evaluation system; it is just a general form in the GM method.

$$\hat{X}^{(1)}(k+1) = \left(X^{(0)}(1) - b_1/a_1\right)e^{-a_1 k} + b_1/a_1 \quad (k = 1, 2, \ldots, m-1) \tag{19}$$

$$\hat{X}(k+1) = \hat{X}^{(1)}(k+1) - \hat{X}^{(1)}(k) \tag{20}$$

Table 6
The eigen-parameters and the predicted values of the GM(1,1) model for the phosphate iron lithium-ion battery under two BEV working mode.

Testing item	a_1	b_1	a_2	b_2	Prediction result of the cycle numbers	Actual cycle number to life ending	Error (%)	AR (%)
30 °C–2 C–100% DoD	0.1123	−41.3434	−0.036	33.0749	4974	5039	1.29	11
50 °C–2 C–100% DoD	−0.0596	6.9872	0.0047	8.6468	570	589	3.22	26

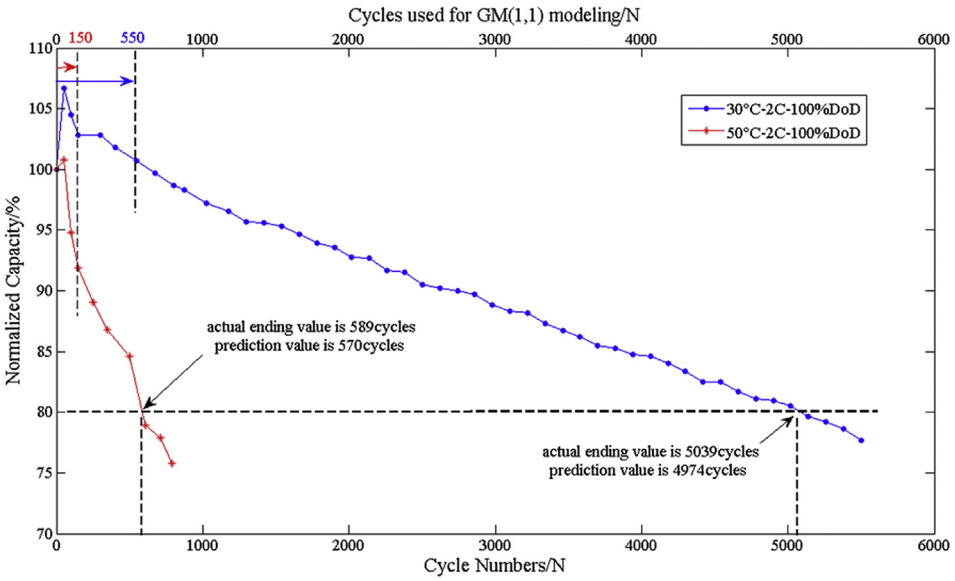

Fig. 8. The actual cycle life profiles of phosphate iron lithium-ion batteries operating under two different BEV modes. The upper horizontal axis is the cycle samples used for GM (1, 1) modeling, which is marked by the arrow. Based on these small amounts of cycle life samples, the predicted value of the battery cycle life can be obtained by the residual GM (1, 1) model. The predicted battery cycle life and the actual value, which corresponds to the 80% of the initial capacity, are both marked.

where $\widehat{x}(k)$ is the prediction value series.

(4) Use a model that has been established, such as Eq. (19) and Eq. (20), to predict the values that have the same serial number as the sample data for the GM (1, 1) modeling. The error between the actual value $X(0)$ and the predicted value $\widehat{X}$ is set to $e^{(0)}$.

$$e^{(0)} = X^{(0)} - \widehat{X} \tag{21}$$

where the absolute value of e will increase as the accelerated aging proceeds because the new trend will be incorporated into the time series. Thus, the next step is aimed at modeling this part of the error for compensating the information contained in the new trend.

(5) Establish the GM (1, 1) model for the error e between the actual value and the prediction value by a similar method as that described in steps (1)–(4), which contain the new trend of the error time series.

$$\widehat{e}^{(1)}(k+1) = \left(e^{(0)}(1) - b_2/a_2\right)e^{-a_2 k} + b_2/a_2 \quad (k = 1, 2, \ldots, m-2) \tag{22}$$

$$\widehat{e}(k+1) = \widehat{e}^{(1)}(k+1) - \widehat{e}^{(1)}(k) \tag{23}$$

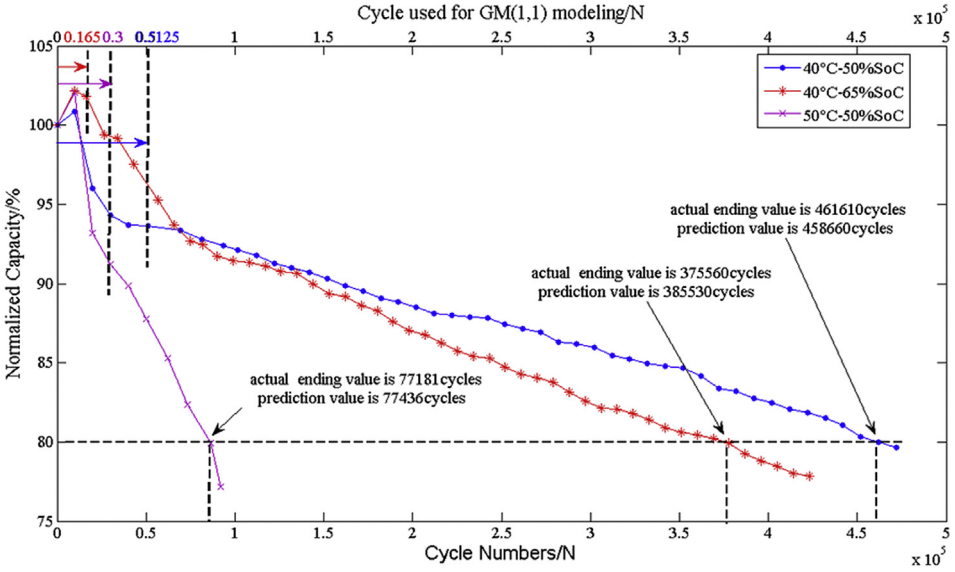

Fig. 9. The actual cycle life profiles of phosphate iron lithium-ion batteries operating under three different HEV modes. The axes and marks in this figure are identical to those of Fig. 8.

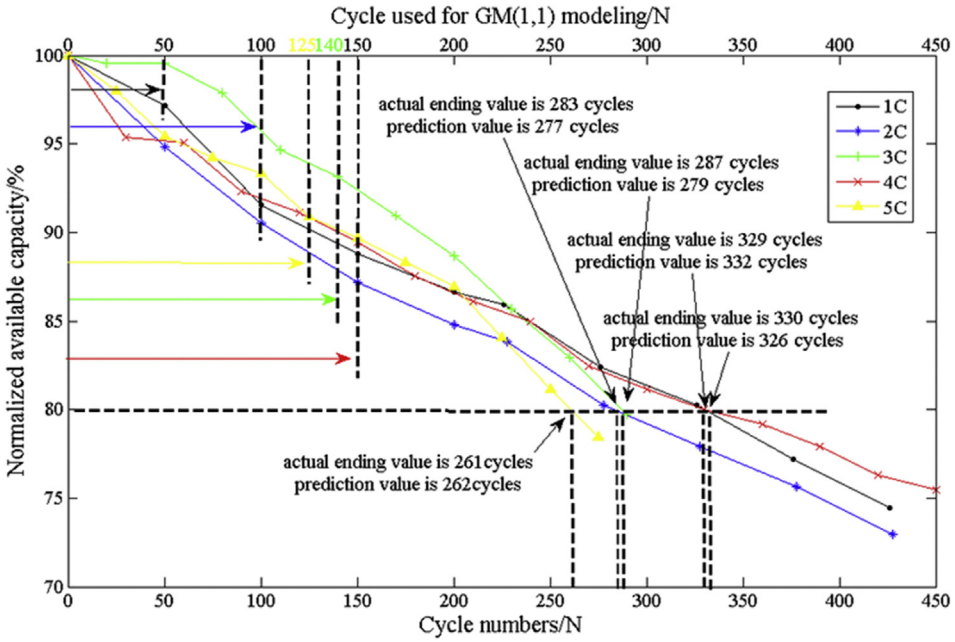

Fig. 10. The actual cycle life profiles of manganese oxide lithium-ion batteries operating under different discharge rates for the BEV mode. The axes and marks in this figure are identical to those of Fig. 8.

(6) Combining Eq. (20) and Eq. (23) yields Eq. (24):

$$\widehat{X}^{(0)} = \widehat{X} + \widehat{e} \tag{24}$$

In this combined model, the first part has the ability to describe the development trend of the time series, and the second part contains the new trend with the sustaining effects of the coupling external impact factors.

(7) Validation of the accuracy of the combined model by examining the error between the predicted value of the cycle numbers of the specified life ending index, such as 80% of the initial capacity, and the real value of the experiment. Note that the prediction value is the square of the model output because the time series used in the modeling is the square root of the raw sequence, as described in step (2). If the accuracy is not satisfied by the initial value of the AR pre-set in step (1), the step is shifted to step (1) to add extra sampling data, adjust the data pre-processing method, reset the expected initial AR value and repeat steps (2)–(7) until the accuracy of the combined model achieves the expectation.

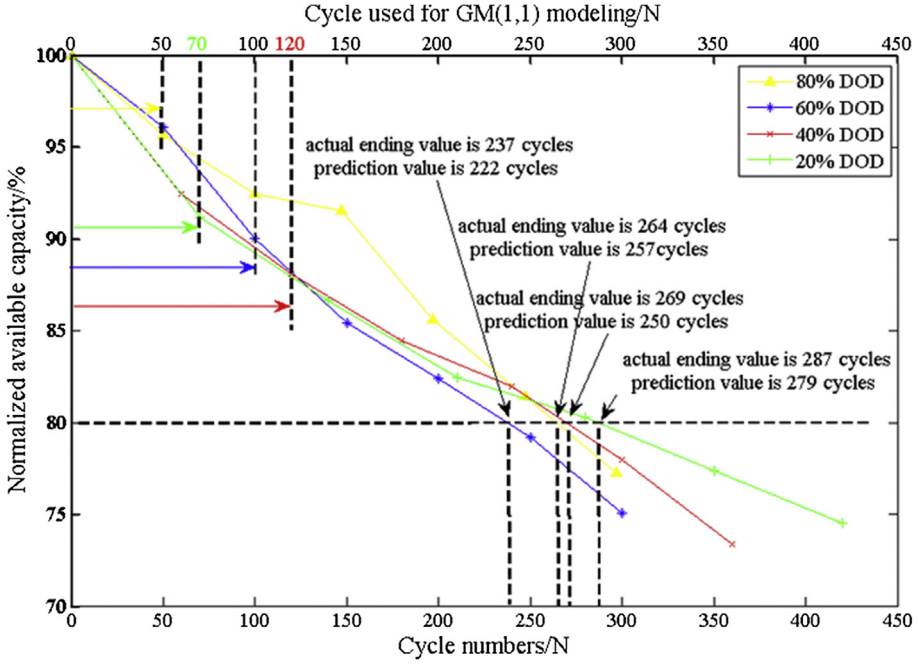

Fig. 11. The actual cycle life profiles of the manganese oxide lithium-ion batteries operating under different DoDs for the BEV mode. The axes and marks in this figure are identical to those of Fig. 8.

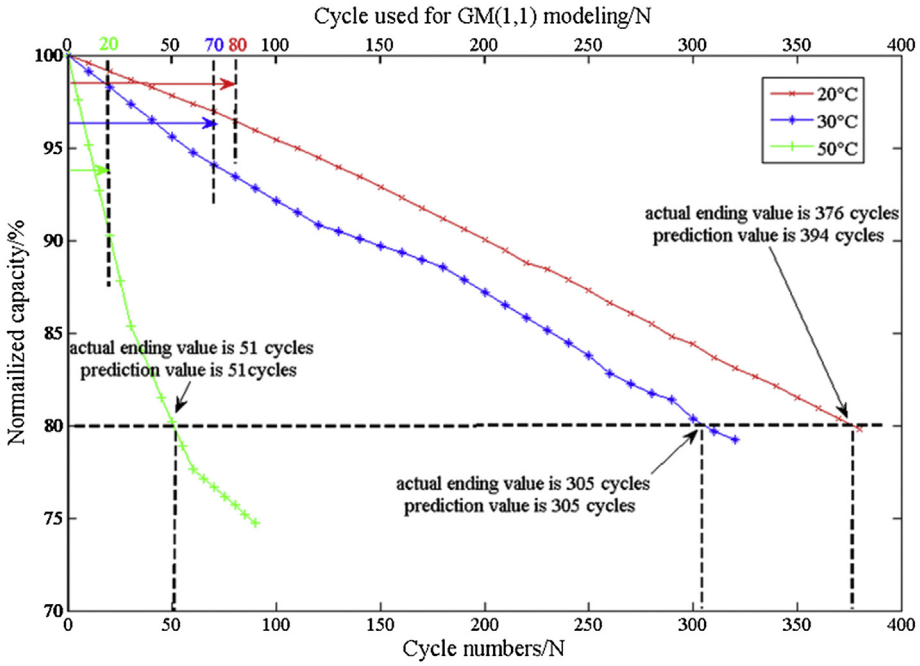

Fig. 12. The actual cycle life profiles of manganese oxide lithium-ion batteries operating under different ambient temperatures for the BEV mode. The axes and marks in this figure are identical to those of Fig. 8.

Table 7
The eigen-parameters and the predicted values of the GM(1,1) model for the phosphate iron lithium-ion battery under three HEV working mode.

Testing item	a_1	b_1	a_2	b_2	Prediction result of the cycle numbers	Actual cycle number to life ending	Error (%)	AR (%)
40 °C–50% SoC	−0.0958	90.1318	0.0054	202.4485	458,660	461,610	0.64	11.1
40 °C–65% SoC	0.0599	−594.7212	0.0040	−27.9937	385,330	375,560	2.6	4.39
50 °C–50% SoC	−0.0751	92.3627	0.0027	248.6837	77,436	77,181	0.33	38.87

4. Results and discussion

4.1. The results analysis of the cycle number prediction

Based on the modeling process for accelerated life testing, as described in Section 3.4, and the testing protocols, as described in Section 2, the GM(1,1) model is established for each testing items by the following means. First, we pre-set the expected value of the initial AR according to the performance index supplied by the battery producer, and then collect the sample data for GM (1, 1) modeling with the accelerated life testing. For example, the data-sheet supplied by the cooperating enterprise indicate that the cycle numbers of the phosphate iron lithium-ion battery in our study exceed 6000 cycles under ambient temperature. According to this suggestion, the value of the initial AR is preset to approximately 10% of the desired accelerated target when we use the testing item specified as the 30 °C, 2 C discharge rate and 100% of the DoD. Thus, we just sampled the performance data within the 550 cycles for GM (1, 1) modeling. Relying on these testing samples, the predicted value of the battery cycle life is 4974 cycles for this testing item, and the detailed value of parameters a_1, b_1, a_2, b_2 in our study are all listed in Table 6. Concurrently, the entire cycle performance profile of this phosphate iron lithium-ion cell proceeds continuously, as shown in Fig. 8, in which we observe the actual cycle number to achieve its life ending state (80% of the initial capacity) is nearly 5039 cycles. The error between the actual cycle number and the predicted value is approximately 1.29%, and the required number of tests has been reduced to 11% of the complete cycle life testing, which saves approximately 4500 cycles.

As for the other single cell of the phosphate iron lithium-ion battery working under the more severe working conditions of 50 °C, 2 C discharge rate and 100% of the DoD, given that the cycle life will be reduced greatly under such severe working conditions and that the battery performance is more sensitive to the influence

Table 8
The eigen-parameters and the predicted values of the GM(1,1) model for the Manganese oxide lithium-ion battery under different discharge rate for EV working condition.

Testing item	a_1	b_1	a_2	b_2	Prediction result of the cycle numbers	Actual cycle number to life ending	Error (%)	AR (%)
100% DoD–40 °C–1 C	0.0488	−24.8554	−0.0442	−0.8002	326	330	1.2	15
100% DoD–40 °C–2 C	0.0173	−49.9724	0.0032	8.3467	277	283	2.1	35
100% DoD–40 °C–3 C	0.0425	−23.4709	0.0145	10.5904	279	287	2.78	48
100% DoD–40 °C–4 C	0.0618	−46.9396	0.0107	13.2737	332	329	0.9	48
100% DoD–40 °C–5 C	0.086	−32.8737	−0.0637	−1.5814	262	261	0.39	48

Table 9
The eigen-parameters and the predicted values of the GM(1,1) model for the Manganese oxide lithium-ion battery under different DoD for EV working condition.

Testing item	a_1	b_1	a_2	b_2	Prediction result of the cycle numbers	Actual cycle number to life ending	Error (%)	AR(%)
20% DOD–40 °C–1 C	0.000376	−202.0788	0.00001487	106.354	279	287	2.78	24
40% DOD–40 °C–1 C	0.0131	−59.659	0.0008637	12.768	250	269	7	48
60% DOD–40 °C–1 C	0.0205	−36.9697	0.0056	11.9822	222	237	6.3	42
80% DOD–40 °C–1 C	0.0488	−25.3826	−0.0441	−0.8171	257	264	2.65	19

Table 10
The eigen-parameters and the predicted values of the GM(1,1) model for the Manganese oxide lithium-ion battery under different ambient temperature for BEV working condition.

Testing item	a_1	b_1	a_2	b_2	Prediction result of the cycle numbers	Actual cycle number to life ending	Error (%)	AR (%)
100% DoD–20 °C–1 C	0.0696	−27.6586	−0.0504	−1.2108	394	376	4.78	21
100% DoD–30 °C–1 C	0.037	−31.0989	0.0106	3.1791	305	305	0	23
100% DoD–50 °C–1 C	0.0185	−20.1243	0.0038	5.5451	51	51	0	39

of the external environment than under soft working conditions, the sampling interval is reduced and the value of AR is increased relatively compared with the previous test battery case. Specifically, the performance data for modeling is sampled at the 1st, 50th, 100th and 150th cycle, and the predicted cycle life obtained from these samples is 570 cycles. The entire performance profile is shown in Fig. 9, in which the actual cycle numbers to reach the life ending condition is 589 cycles. Thus, the required number of tests has been reduced to 26% of the complete cycle life testing, which saves approximately 420 cycles. And the error between the actual cycle number and the prediction value is approximately 3.22%. The detailed model parameters are also listed in Table 6. Note that the capacity of the lithium iron phosphate testing samples used in our study actually increase in the initial few cycles, which may be related to the manufacturing process, such as too large a compaction density or an incomplete formation process. To verify the robustness of our model, we have not performed any modification of the raw sample data.

A similar approach was implemented on other testing samples. For the HEV working mode, the entire life profile of the phosphate iron lithium-ion battery is shown in Fig. 9; the required cycle numbers for the accelerated life testing was greatly reduced, especially for the testing items under 40 °C ambient temperature, and the error does not exceed 3%. The slower decay trend under the HEV operation mode leads to more smooth data samples for GM (1, 1) modeling and the improved effectiveness of our method.

Regarding the manganese oxide lithium-ion battery, the validity of the GM (1, 1) model in the accelerated testing also can be verified by our testing samples used under different conditions, as described in Section 2. Note that the cycle performance of this batch of batteries is not as good, due to their shorter cycle life. However, the reduced cycle performance will not impact the effectiveness of our model, as these volatile data can demonstrate the further applicability of the model to different objects and situations. The cycle life profiles are shown in Fig. 10 to Fig. 12. In detail, the discharge rate effect on the battery cycle life is shown in Fig. 10, and the effects of the DoD and the ambient temperature are shown in Figs. 11 and 12, respectively. The comparison between the actual cycle number achieving the life ending condition and the predicted value is presented in Table 8 to Table 10, and the corresponding model parameters and the results analysis are also listed in these tables. Although the value of AR is larger compared with the phosphate iron lithium-ion battery, the total number is reduced to 29% of the complete accelerated life testing, i.e., the total charge and discharge numbers are reduced from 3686 cycles to 1075 cycles, which is valuable in performing a battery life study.

From these prediction results, the GM (1, 1) accelerated testing model is applicable to the cycle number prediction for various types of lithium-ion battery working conditions, including BEV mode and HEV mode.

4.2. Comparison between the grey method and the conventional method

4.2.1. Comparison from the perspective of the battery life modeling

As for the current battery life models, whatever the mechanism model or data-driven model, the basis of them is usually a large number of testing samples. However, the fading law obtained from these models may be not applicable for other types of lithium ion battery, even for those that own the same material systems.

For instance, the models suggested in the [8–11] indicate the fading trend of their testing lithium-ion battery is satisfied the square-root law. And according to the related documents, this conclusion is mainly based on the assumption that the fading of the lithium-ion battery is caused by the SEI, and the velocity of the SEI growth accords to the square-root law [18]. However, it may be not a general conclusion due to the complicated and coupled fading mechanism besides the SEI growth, and the exclusive additives within the battery component may affect the battery physical and chemical properties on different life stage.

And then, we obtained the fading law of our testing samples according to the model structure and modeling process in Ref. [8]. The fitting results indicate that the power function is good to describe the relationship between the capacity fading and the use time, but the order of the use time is not always 0.5. The fitting results for different working conditions are listed in Tables 11–15, it is farfetched to ascribe the fading of all lithium ion battery to a fixed law.

Table 11
The fitting results of the conventional battery life model for the Manganese oxide lithium-ion battery under different discharge rate for BEV working condition.

Working condition	The order of the use time
100% DoD–40 °C–1 C	0.9512
100% DoD–40 °C–2 C	0.7521
100% DoD–40 °C–3 C	1.62
100% DoD–40 °C–4 C	0.7139
100% DoD–40 °C–5 C	0.8883

Table 12
The fitting results of the conventional battery life model for the Manganese oxide lithium-ion battery under different DoD for BEV working condition.

Working condition	The order of the use time
80% DoD–40 °C–1 C	0.8796
60% DoD–40 °C–1 C	1.004
40% DoD–40 °C–1 C	0.6821
20% DoD–40 °C–1 C	0.5853

By comparison, our method obtains the model parameters by an identification technique and own good accuracy, which is not a fixed model structure for battery life prediction. The parameter and the prediction accuracy have been listed in Tables 8–10. Thus compared with the conventional battery life model, the advantage of our method for battery life model mainly include the below two aspects. Firstly, no requirements for pre-knowledge of battery fading mechanism and small data samples and owns higher prediction accuracy. Secondly, the parameter is self-adaptive for different working condition, and the model owns the ability to praise the battery performance for a random usage condition.

4.2.2. Comparison from the perspective of the accelerating life test

Usually, acceleration test of capacity fade was used for prediction of the fade value. As for the testing technique, our method presents a convenient method to accelerate the conventional battery life test. By our method, we reduce the testing time through predicting the number of cycles that achieve a random life ending index based on a small number of testing samples. And the predicted value can be used to battery life modeling on the cost of little loss of prediction accuracy. In detail, the modeling samples are the prediction results from our method, which just requires a small number of actual testing results, and the model structure is referred to a conventional battery life model.

Take the phosphate lithium-ion battery that worked under two BEV mode for examples, the modeling samples comes from our GM(1,1) model and parameters of the GM(1,1) model have been listed in Table 6, and the life model structure is referred to that established by Bloom in Ref. [8].

And then, the battery life model for these two BEV mode are expressed as Eq. (25) and Eq. (26). Eq. (25) corresponds to the working condition of 30 °C–2 C–100% DoD, and Eq. (26) corresponds to the working condition of 50 °C–2 C–100% DoD.

$$\text{Capacity} = 8.72 \times \left[1 - \exp(-5.98) \times t^{0.481}\right] \tag{25}$$

$$\text{Capacity} = 8.398 \times \left[1 - \exp(-6.155) \times t^{0.7306}\right] \tag{26}$$

where symbol capacity is the actual battery capacity, t is the use time.

And the comparison between the prediction value of life model and the testing results is shown in Fig. 13 and Fig. 14. From the two figures, we can conclude that the battery life model based on the prediction value of GM (1, 1) method owns higher accuracy and reduces the required testing time to a small level, which has been reduced to 11% and 26% for these two working conditions as listed in Table 6.

Similarly, just like the summary in Section 4.1, the whole testing items for Manganese oxide lithium-ion battery can meet the requirements of the most conventional battery life modeling method. And as the discussion on the Section 4.1, the accelerated method of our study can reduce the testing time nearly to 29% of the whole testing time.

Table 13
The fitting results of the conventional battery life model for the Manganese oxide lithium-ion battery under different ambient temperature for BEV working condition.

Working condition	The order of the use time
100% DoD–20 °C–1 C	1.126
100% DoD–30 °C–1 C	0.7557
100% DoD–50 °C–1 C	0.5105

Table 14
The fitting results of the conventional battery life model for the phosphate iron lithium-ion battery under two BEV working condition.

Working condition	The order of the use time
30 °C–2 C–100% DoD	0.4795
50 °C–2 C–100% DoD	0.5516

4.3. Analysis of the capacity fade characteristic

4.3.1. Effect of DoD on the battery capacity fade

From the testing results of this paper, the battery fading will be accelerated by the increase of the DoD, but this trend is not so obvious for our testing samples.

By the comparison of the parameters of our method can deliver some useful information about the effect of DoD on the aging character of the lithium-ion battery. In our method, a_1 and b_1 model the raw performance data, while a_2 and b_2 just model the prediction error. Thus it is more suitable using parameter a_1 and b_1 to study the relationship between the external impact factor and internal fading law.

As discussed in Section 3.2.1, parameter a_1 show the development trend of raw data, which describes the fading trend of the testing samples; b_1 represents the influence of the external disturbance, which can be used to interpret the effect of each impact factor on battery life. The detailed value of a_1 and b_1 for the Manganese oxide lithium-ion battery under different DoD have been listed in Table 9. Based on the definition of GM(1,1) model, i.e. Fig. 6 and Eq. (1), we can get that the raw data should be smaller when the value of a_1 is lager, but the development trend is also influenced by parameter b_1, which act as a compensation variable. The larger absolute value of b_1 means the development of raw data is more susceptible to the external condition. Just like Table 9 shown, with the increase of DoD, the value of a_1 will be increasing and the number of cycles will be decreasing to some extent. But due to the compensation of parameter b_1, the difference of the battery cycle life under different DoD is not so obvious. Thus we conclude that DoD will affect the cycle life of our testing samples but there exists some complicated mechanism restrain the loss of the capacity, thus the fading law is not so sensitive to the value of DoD.

Table 15
The fitting results of the conventional battery life model for the phosphate iron lithium-ion battery under three HEV working condition.

Working condition	The order of the use time
40 °C–50% SoC	0.3662
40 °C–65% SoC	1.53
50 °C–50% SoC	0.5273

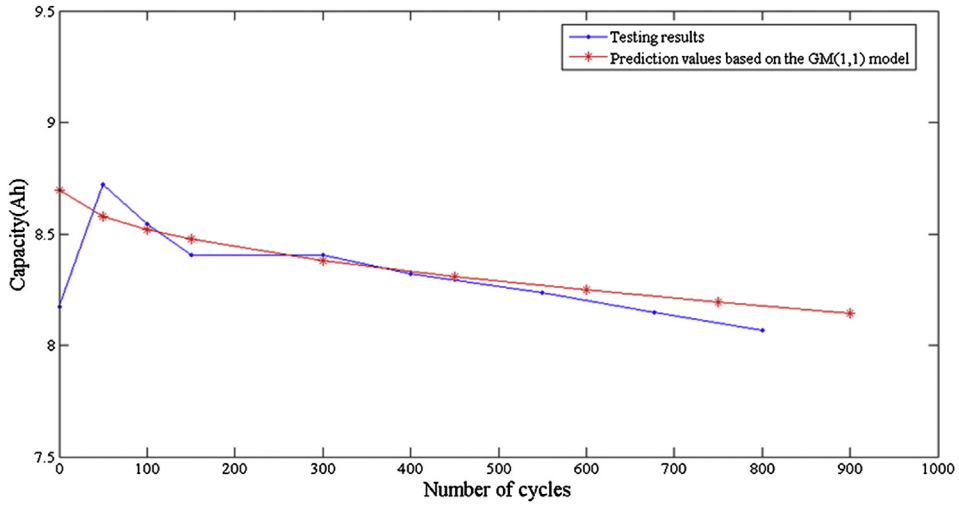

Fig. 13. The comparison between the prediction value of life model based on the GM(1,1) model and the actual testing results. (30 °C–2 C–100% DoD).

4.3.2. Effect of cathode materials on capacity fading

There have many differences between cathode and anode. For instance, SEI film plays an important role in the anode and its change will affect the anode performance, but the performance of the cathode is primarily related to the cathode material. Different cathode materials own different chemical and physical properties. For instance, the Mn^{2+} dissolution reaction and the structure defects caused by the Jahn–Teller distortion are the primary capacity fading reason for the Manganese oxide lithium-ion battery [19]. But due to the difference of the thermodynamics and lattice characters, the similar phenomenon has seldom happened in the Phosphate lithium-ion battery, thus the rate of the capacity fading is slower than the Manganese oxide lithium-ion.

For our method, we can also get some information from the model parameter a_1 and b_1 to compare the fading law of the lithium-ion battery with different cathode material. By the comparison between Tables 6–7 and Tables 8–10, it can be seen that the value of a_1 of the Phosphate lithium-ion battery is smaller than that of Manganese oxide lithium-ion battery. According to the meaning of a_1, we can get that the cycle life of Phosphate iron lithium-ion battery is longer than the manganese oxide lithium-ion battery. And the dispersion of parameter b_1 is more obvious for Phosphate iron lithium-ion battery, which suggests that the capacity fading of the Phosphate iron lithium-ion battery is more easily affected by the external factor such as temperature and SoC. This also means that temperature and SoC are the effective accelerating factors in battery life test design for the Phosphate iron lithium-ion battery.

4.3.3. Relationship between the calendar loss and the cycle loss

A valuable capacity fading model should cover the calendar loss and cycle loss. There have been lot of achievements on the cycle life or calendar life of the lithium-ion battery, but there was no unified conclusion on the relationship between these two fading mode and the corresponding internal mechanism. Thus we just discuss this issue according to the results of our method.

Firstly, we compare the results of the phosphate lithium ion battery that worked under the BEV mode (50 °C–2 C–100% DoD) and the HEV mode (50 °C–50% SoC) for their identical ambient temperature and the approximate average current rate. And there have 1 h rest time between each charge and discharge stage for BEV mode, but HEV mode no. As listed in Tables 6 and 7, there has obvious difference for parameter b_1 for these two working conditions, which means that the rest time will affect the battery life to some extent. And this phenomenon has been mentioned in Section 3.1, and Fig. 4(a) has indicated this difference.

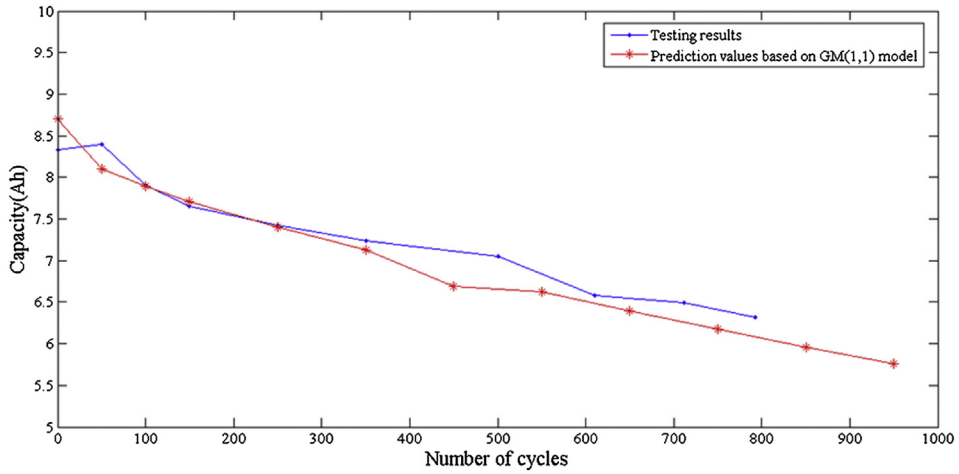

Fig. 14. The comparison between the prediction value of life model based on the GM(1,1) model and the actual testing results. (50 °C–2 C–100% DoD).

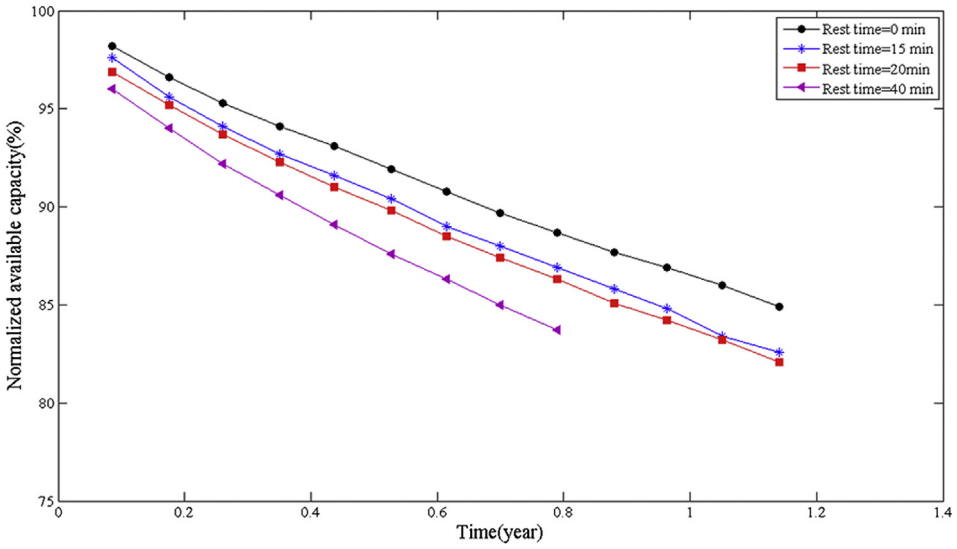

Fig. 15. Comparison of the capacity fading trend working under the conditions with different rest time in minutes between charge and discharge half-cycles.

In order to further study this difference, we refer to the literature [20], which concludes that the fading rate is the lowest with no rest time, and the fading rate increase with the longer rest times. As drawn in Fig. 15, this conclusion is also suitable for our testing samples, and Table 16 gives out the predicted value and the identified parameters of our model. From these parameters, we can see that the difference of b_1 will be greater with the rest time increase, which indicate that the fading trend is influence by the rest time. And parameter a_1 with the rest time are all bigger than that of the working condition with no rest time, that indicates the usable life of the lithium-ion battery are reduced with the appearance of the rest time.

The above results show that the battery fading will be accelerated when the rest time appeared in the continuous charge and discharge process. And this trend will be more impressive with the rest time increased. Thus a valuable research on the battery life in the vehicle application should integrate the calendar loss into the cycle loss.

5. Conclusions

A data-driven model used to reduce the cycle numbers for the life testing of lithium-ion batteries was presented in this paper. According to this model, a small amount of data is required to achieve the accelerated battery life testing. The accuracy of this method is verified by predicting the cycle life of two commonly used battery material systems; the results demonstrated that this method is helpful for solving the issues confronted in performing the life study, such as the lack of data samples and the time-consuming nature of the life testing. Although the battery cycle life can be predicted, our model is not a cycle life model, strictly speaking, due to the variable eigen-parameters used, which have no fixed rules for each working condition.

Table 16
The eigen-parameters and the predicted values of the GM(1,1) model for the lithium-ion battery with different rest time.

Working condition	a_1	b_1	a_2	b_2	Actual life	Prediction result
Rest time = 0(min)	0.053	−2.6022	−0.0250	−0.1163	1.6584	1.6391
Rest time = 15(min)	0.0594	−2.6926	0.0466	−0.1421	1.6482	1.6372
Rest time = 20(min)	0.0617	−2.7229	0.0196	−0.1221	1.5147	1.5177
Rest time = 40(min)	0.059	−3.2135	0.0281	−0.1105	1.2677	1.2603

Acknowledgment

This work is financially supported by the Major State Basic Research Development Program of China (973 Program, Grant No. 2011CB711202), the National Natural Science Foundation of China (NSFC, Grant No. 51207111), and the Specialized Research Fund for the Doctoral Program of Higher Education (SRFDP, Grant No. 20130072110055).

References

[1] M. Conte, F.V. Conte, I. Bloom, K. Morita, I. Tomohiko, J. Belt, in: The 25th World Battery, Hybrid and Fuel Cell Electric Vehicle Symposium & Exhibition, Shenzhen, China, 2010.
[2] P. Ramadass, B. Haran, P.M. Gomadam, R. White, B.N. Popov, J. Electrochem. Soc. 151 (2004) A196.
[3] S. Sankarasubramanian, B. Krishnamurthy, J. Electrochim. Acta 70 (2012) 248–254.
[4] G. Ning, R.E. White, B.N. Popov, J. Electrochim. Acta 51 (2006) 2012–2022.
[5] G. Ning, B.N. Popov, J. Electrochem. Soc. 151 (2004) A1584.
[6] V. Srinivasan, J. Newman, J. Electrochem. Soc. 151 (2004) A1517.
[7] J. Newman, W. Tiedemann, AIChE J. 21 (1975) 25–41.
[8] I. Bloom, B.W. Cole, J.J. Sohn, S.A. Jones, E.G. Polzin, V.S. Battaglia, G.L. Henriksen, C. Motloch, R. Richardson, T. Unkelhaeuser, D. Ingersoll, H.L. Case, J. Power Sources 101 (2001) 238–247.
[9] J. Wang, P. Liu, J. Hicks-Garner, E. Sherman, S. Soukiazian, M. Verbrugge, H. Tataria, J. Musser, P. Finamore, J. Power Sources 196 (2011) 3942–3948.
[10] E.V. Thomas, I. Bloom, J.P. Christophersen, V.S. Battaglia, J. Power Sources 206 (2012) 378–382.
[11] R.B. Wright, C.G. Motloch, J.R. Belt, J.P. Christophersen, C.D. Ho, R.A. Richardson, I. Bloom, S.A. Jones, V.S. Battaglia, G.L. Henriksen, T. Unkelhaeuser, D. Ingersoll, H.L. Case, S.A. Rogers, R.A. Sutula, J. Power Sources 110 (2002) 445–470.
[12] H. Dai, X. Wei, Z. Sun, J. Wang, W. Gu, Appl. Energy 95 (2012) 227–237.
[13] E.V. Thomas, I. Bloom, J.P. Christophersen, V.S. Battaglia, J. Power Sources 184 (2008) 312–317.
[14] W.C. Wong, J. Newman, J. Electrochem. Soc. 149 (2002) A493.
[15] M. Ecker, J.B. Gerschler, J. Vogel, S. Käbitz, F. Hust, P. Dechent, D.U. Sauer, J. Power Sources 215 (2012) 248–257.
[16] S. Liu, J. Grey Syst. UK 2 (2007) 111–123.
[17] D. Julong, J. Grey Syst. UK 1 (1989) 1–24.
[18] Advances in Lithium-ion Batteries, Kluwer Academic Publishers, New York, 2002.
[19] J. Vetter, P. Novák, M.R. Wagner, C. Veit, K.C. Möller, J.O. Besenhard, M. Winter, M. Wohlfahrt-Mehrens, C. Vogler, A. Hammouche, J. Power Sources 147 (2005) 269–281.
[20] J. Belt, V. Utgikar, I. Bloom, J. Power Sources 196 (2011) 10213–10221.